

## Robust control approach to force estimation in a constant position optical tweezers

Tanuj Aggarwal, Hullas Sehgal, and Murti Salapaka

Citation: *Rev. Sci. Instrum.* **82**, 115108 (2011); doi: 10.1063/1.3660271

View online: <http://dx.doi.org/10.1063/1.3660271>

View Table of Contents: <http://rsi.aip.org/resource/1/RSINAK/v82/i11>

Published by the [American Institute of Physics](#).

---

### Related Articles

Optofluidic cell manipulation for a biological microbeam

*Rev. Sci. Instrum.* **84**, 014301 (2013)

Combined versatile high-resolution optical tweezers and single-molecule fluorescence microscopy

*Rev. Sci. Instrum.* **83**, 093708 (2012)

Single-cell adhesion probed in-situ using optical tweezers: A case study with *Saccharomyces cerevisiae*

*J. Appl. Phys.* **111**, 114701 (2012)

Absolute calibration of optical tweezers including aberrations

*Appl. Phys. Lett.* **100**, 131115 (2012)

Three dimensional optical twistors-driven helically stacked multi-layered microrotors

*Appl. Phys. Lett.* **100**, 121101 (2012)

---

### Additional information on *Rev. Sci. Instrum.*


Journal Homepage: <http://rsi.aip.org>

Journal Information: [http://rsi.aip.org/about/about\\_the\\_journal](http://rsi.aip.org/about/about_the_journal)


Top downloads: [http://rsi.aip.org/features/most\\_downloaded](http://rsi.aip.org/features/most_downloaded)

Information for Authors: <http://rsi.aip.org/authors>

## ADVERTISEMENT



Does your research require low temperatures? Contact Janis today.  
Our engineers will assist you in choosing the best system for your application.



10 mK to 800 K  
Cryocoolers  
Dilution Refrigerator Systems  
Micro-manipulated Probe Stations

LHe/LN<sub>2</sub> Cryostats  
Magnet Systems

[sales@janis.com](mailto:sales@janis.com)   [www.janis.com](http://www.janis.com)  
**Click to view our product web page.**

# Robust control approach to force estimation in a constant position optical tweezers

Tanuj Aggarwal,<sup>a),b)</sup> Hulas Sehgal,<sup>a),c)</sup> and Murti Salapaka<sup>d)</sup>

*University of Minnesota, 200 Union St SE, Minneapolis, Minnesota 55455, USA*

(Received 6 December 2010; accepted 19 October 2011; published online 22 November 2011)

Feedback enhanced optical tweezers with position regulation capability enable detection and estimation of forces in the pico-Newton regime. In this article we delineate the fundamental limitations and challenges of existing approaches for regulating position and force estimation in an optical tweezer. A modern control systems approach is shown to improve the bandwidth of force estimation by three to four times which is corroborated experimentally. © 2011 American Institute of Physics. [doi:[10.1063/1.3660271](https://doi.org/10.1063/1.3660271)]

## I. INTRODUCTION

Single cell and single molecule studies require instruments with the ability to manipulate and interrogate matter at the nanoscale. One of the prevalent means of probing single molecules is optical tweezers<sup>1</sup> that provide the capability of measuring interaction forces with sub pico-Newton resolution.

Optical tweezers use radiation pressure of a focused laser beam to trap and maneuver sub-micron sized dielectric particles (henceforth called beads) with a refractive index higher than that of the surrounding medium. Typically, the molecule under investigation is chemically tethered to a bead that is held in an optical trap.<sup>2</sup> The dynamics of the biomolecule is inferred from the measurements of the position of the trapped bead.<sup>3</sup> Thus, the force measurement resolution is determined by the attainable resolution with which the position of the bead can be determined.

In most current optical tweezers setups, the position of the bead is measured using a position sensitive photodiode,<sup>3</sup> which collects the laser light that passes through the bead. The behavior of an optically trapped bead can be modeled by an overdamped Hookean spring provided the bead stays within a couple of hundred nanometers of the center of the optical trap.<sup>4</sup> More nuanced models that address hydrodynamic effects are presented by Berg-Sørensen and Flyvbjerg.<sup>5</sup> Feedback strategies have significantly enhanced the performance of optical tweezers. The two prevalent feedback modes of optical tweezers operation are: the isotonic clamp<sup>6</sup> and the isometric clamp.<sup>3</sup> Isotonic clamps are particularly useful in measuring the stepping behavior of motor proteins by regulating the force applied by the optical trap and thereby maintaining a constant tension in the protein. Isometric clamps (also called constant position optical tweezers (CPOTs)) regulate the position of the trapped bead to a constant value by changing the position of the trap. In an isometric clamp external forces exerted on the bead are countered by opposing forces exerted by changing the position of the trap. Here, the effort/force

required to regulate the position of the trapped bead is considered to be a direct measure of the force exerted by the biomolecule under investigation. In a detection scheme where the bead position is measured using a stationary reference laser beam separate from the trapping beam, position regulation helps maintain the fidelity of measurements by keeping the trapped bead within the linear detection region of the detection beam.

As noted earlier, in an optical tweezers setup, the force generated by a biomolecule is inferred by a bead tethered to the biomolecule. One of the fundamental limitations on the temporal resolution of the force measurements is imposed by the time constants of the bead dynamics. In other words, force profiles that change faster than the bead's response time cannot be inferred easily from the measurements of the bead position.<sup>7</sup> In a constant position optical tweezers, measurements of the bead position is processed by a controller that manipulates the laser to reposition the bead to a specified location. It can be shown that this strategy of regulating the bead position, together with the interpretation of the control effort as an estimate of the forces, partly overcomes the limitations on the temporal resolution of force estimation imposed by the bead dynamics.<sup>8–10</sup> Effectively, feedback increases the stiffness of the entire system, which improves the temporal resolution of force estimation. In this article we present evidence that the feedback strategy also has limitations in that the effective stiffness cannot be increased indefinitely. We delineate the causes for these limitations. We present experimental evidence that if the proportional gain of a proportional-integral controller is increased beyond a certain threshold, then the power spectral density of the bead position shows a qualitative change,<sup>4,11</sup> wherein a resonance-like peak, that cannot be explained by the first order dynamics of the feedback controlled bead, appears. The changed dynamics, makes the operation non-robust wherein small perturbations destabilize the operation rendering high gain controllers ineffective. Thus, we demonstrate that using the strategy of increasing controller gains precludes achieving high bandwidth force estimation. An instance of the utility of high bandwidth estimation that transcends these limitations is the ability to observe the dynamics of biomolecules under physiological conditions where currently the experiments

<sup>a)</sup>Tanuj Aggarwal and Hulas Sehgal are joint first authors

<sup>b)</sup>Electronic mail: [aggar028@umn.edu](mailto:aggar028@umn.edu).

<sup>c)</sup>Electronic mail: [hulas.sehgal@gmail.com](mailto:hulas.sehgal@gmail.com).

<sup>d)</sup>Electronic mail: [murtis@umn.edu](mailto:murtis@umn.edu).

are conducted under non-physiological conditions achieved by reducing ATP concentration.<sup>3</sup> In this article we address the question, whether it is possible to use optical tweezers for measuring forces having high frequency content by employing a linear feedback strategy while avoiding problems such as emergence of a peak in the power spectrum of the bead position. This question is addressed in Sec. IV of this article, where fundamental limitations arising due to latencies<sup>4,11</sup> in the closed loop optical tweezers are discussed.

High bandwidth estimation using optical tweezers was reported earlier by the authors using an inversion based approach that resulted in an order of magnitude increase in the bandwidth of external force estimation.<sup>7</sup> The reported scheme utilizes a PI controller for position regulation followed by an *ad hoc* inversion of the experimentally identified dynamical map from external force to measured output. However, the scheme is restricted by the PI controller structure. In this article the problem of estimating forces with high bandwidth is cast in a robust control framework wherein multiple objectives of constant position regulation of the trapped bead and estimation of external force are optimized simultaneously over the space of all stabilizing controllers. We show an improved bandwidth of force estimation over the system inversion strategy<sup>7</sup> and also provide the limits of achievable performance using the linear control strategies. Results are verified through simulations and demonstrated experimentally.

Our experimental setup of CPOT is presented in Sec. II. The modeling of CPOT from a control systems perspective is described in Sec. III, followed by an explanation of fundamental limitations that plague the closed loop operation of optical tweezers in Sec. IV. The challenge of increasing the bandwidth of a constant position optical tweezers is dealt with in the robust control framework in Sec. V where an optimal linear feedback strategy is developed to measure external forces having high frequency content. Finally, the experimental results are presented in Sec. VI.

## II. EXPERIMENTAL SETUP

Figure 1 shows the schematic of optical tweezers setup along with the detection and feedback mechanism. The linearly polarized IR laser beam (Nd:YAG laser from Crysta-Laser Inc.,  $\lambda = 1064$  nm, maximum power output = 500 mW) is expanded using a 10 $\times$  beam expander (Thorlabs Inc.) and passed through a half-wave plate that rotates the polarization vector such that most of the power is along the s-polarized (s-pol) component and only a small percentage of the total laser power is in the p-polarized (p-pol) component. A polarizing beam splitter (PBS1, Newport Inc.) splits these components spatially by allowing transmission of the p-pol while reflecting the s-pol (45° angle of incidence), thereby creating two non-interfering beams. The s-pol beam is used for creating the trap whereas the p-pol beam is used for detection of the trapped bead. The p-pol beam is used for detection since the s-pol beam has smaller leakage through PBS1. It is seen that PBS1 allows 0.01% transmission of s-pol beam while allowing 4% reflection of the p-pol beam which results in a small amount of coupling.

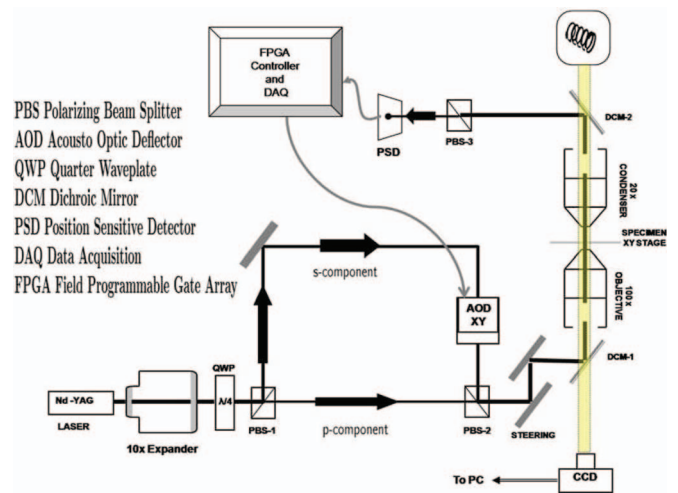


FIG. 1. (Color online) Schematic of our optical tweezers setup outlining the detection and actuation mechanism. The solid black line represents the laser path with the arrows indicating the direction of propagation. The laser source emits linearly polarized beam. The beam's polarization vector is rotated using a half-wave plate before it enters a polarizing beam splitter (PBS-1). PBS-1 splits the s and p components of the polarized beam to create two orthogonally polarized beams. The s-polarized beam is sent through a dual-axis AOD and forms the high intensity trap. p-polarized beam is low intensity and is used for detection purposes. Both the beams are nominally collocated at the specimen plane. The fluctuations of the trapped bead are measured by imaging the p-polarized beam, that passes through the bead, onto the position sensitive photodiode (PSD). The AOD is computer controlled, thus enabling modulating the optical trap due to the s-polarized beam.

The s-pol beam is passed through a dual axis acousto-optic deflector, AOD (IntraAction Corp. DTD-276HD6) before it is combined with the p-pol beam at the beam splitter, PBS2. The combined beam is introduced into the inverted microscope (Nikon Inc., TE2000U) from above the epi-fluorescence port and directed into the back aperture of the oil immersion objective (numerical aperture, NA = 1.4) using the dichroic mirror, DM1. The power of p-pol beam is reduced to an extent that it has negligible effect on the optical trap. The sample for our experimental results is a colloidal solution of polystyrene beads, 2.1  $\mu\text{m}$  in diameter. Both the p-pol and the s-pol beams are passed through separate telescopic arrangements of plano-convex lenses (not shown in the figure). The telescopic lenses in the s-pol beam path have focal lengths matched to make the AOD output plane conjugate to the back focal plane of the microscope objective. This ensures that changing the trap position does not change the trap symmetry.

The detection setup consists of a 20 $\times$  objective mounted above the sample stage on a manual X–Y–Z micropositioner. It serves the dual purpose of condensing the light from the halogen lamp used for illuminating the sample and for collecting the laser beam exiting from the sample. The dichroic mirror DM2 directs the collimated laser beam exiting the condenser objective to a third beam splitter, PBS3. PBS3 splits the p- and s-polarized beams. The p-polarized beam is directed to a position sensitive photodetector (PSD) (Pacific Silicon Sensor Inc., DL100-7PCBA3) while the high power s-polarized beam is collected in a beam dump. A FPGA based data acquisition system (National Instruments, PCI 7833R)

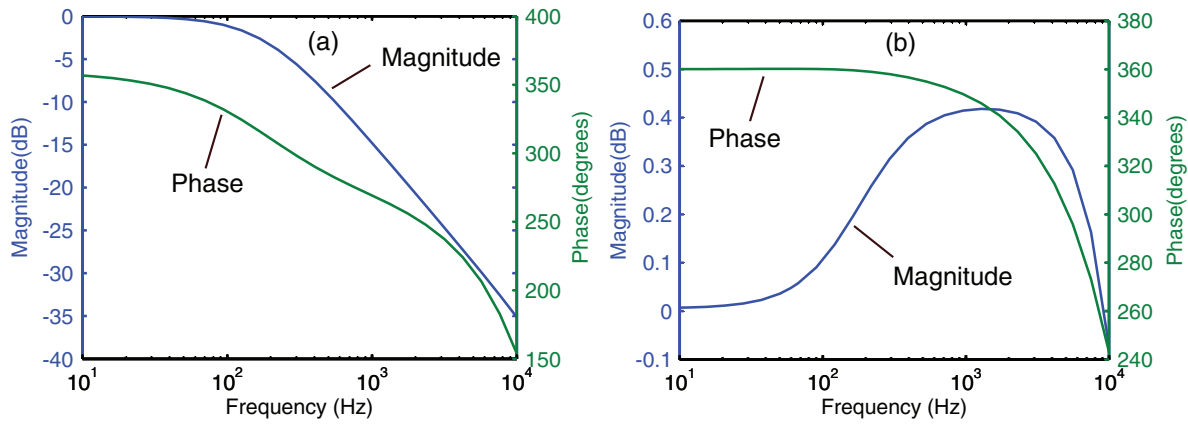


FIG. 2. (Color online) (a) Experimentally determined frequency response of the transfer function,  $H = GD$ , of the optical tweezers system. Input of  $H$  is the command,  $\tilde{u}$ , given to the AOD and the output of  $H$  is the measurement,  $y$ , from the photodiode. Magnitude curve is the magnitude of amplification of inputs at the output whereas the phase curve characterizes the delay between the input and the output. (b) Frequency response of the transfer function of the instrumentation dynamics,  $D$ , deduced from  $H$  and a physical model,  $G$ , of the bead dynamics in an optical trap.

is used to capture voltage signals from the photodiode and to implement a real-time digital feedback controller in LabVIEW (National Instruments). The controller output actuates the trap position by modulating the input to the AOD. A colored charged couple device (CCD) camera is used to view the specimen on the computer. The optical setup is mounted on an air table (Melles Griot Inc.) to isolate it from ground vibrations. The optics of the detection system are mounted on a custom made aluminum optical breadboard.

### III. MODELING CONSTANT POSITION OPTICAL TWEEZERS

#### A. Physical model

The optically trapped bead system is typically modeled as a linear spring-mass-damper system for relatively small displacements of the trapped bead from the trap position.<sup>12</sup> Equation of motion (EOM) governing this behavior is given by,

$$\beta \dot{x} + k(x - u) = \eta(t) + F_e(t), \quad (1)$$

where  $\beta$  is the damping coefficient,  $\eta$  is the stochastic Langevin force (thermal noise),  $F_e$  denotes the sum of all external forces,  $x$  is the instantaneous position of the bead,  $u$  is the instantaneous position of the laser trap, which is controlled by the AOD, and  $k$  is the trap stiffness constant. The EOM relates the net force ( $F_e + \eta$ ) on the trapped bead to the bead position ( $x$ ). EOM in Eq. (1) can be viewed as an input-output system with the force as the input and the bead position as the output. This model suffers from undermodeling due to lack of accountance of hydrodynamic interactions. A more complete model by Berg-Sørensen and Flyvbjerg<sup>5</sup> may be used but it is not amenable to the analysis in this article. Input-output relations that are governed by ordinary differential equations are conveniently handled in the Laplace transform domain where the Laplace transform of Eq. (1) is given by

$$x(s) = \frac{k}{\beta s + k} u(s) + \frac{1}{\beta s + k} (\eta(s) + F_e(s)), \quad (2)$$

$s$  being the Laplace transform variable. The Fourier response of the system at any angular frequency  $\omega$  can be obtained by setting  $s = j\omega$ . We define the transfer function,  $G(s) : \frac{x}{u} = k(\beta s + k)^{-1}$  which, for  $s = j\omega$ , represents the frequency response of the system from input  $u(s)$  to output  $x(s)$ . Note that a single-input single-output transfer function only relates effect of one particular input to the output. The net output is the sum of products of transfer functions and corresponding inputs as in Eq. (2). Analyses in the subsequent sections uses the following tools and definitions. The frequency response of the system with transfer function  $G(s)$  consists of two plots: plot of  $20 \log |G(j\omega)|$  and of  $\tan^{-1} G(j\omega)$  with respect to the logarithm of angular frequency,  $\omega$ . It represents the amplification and phase delay, respectively, introduced by the system  $G$  to an input sinusoid of frequency  $\omega$ . The maximum amplification over all the frequencies is the  $H_\infty$  norm of the system, i.e.,  $\|G\|_\infty := \max_\omega |G(j\omega)|$ . The frequency response of an experimentally determined transfer function of an open loop optical tweezers is shown in Fig. 2. Roots of the numerator polynomial of  $G(s)$  are zeros of the system and the roots of the denominator polynomial are the poles of the system. A root with negative real part is referred to as a left half plane (LHP) zero (pole) whereas a root with a positive real part is referred to as the right half plane (RHP) zero (pole). For the remaining discussion, all transfer functions and signals are functions of  $s$  and this argument is dropped for notational convenience. Equation (2) is then rewritten as

$$x = Gu + G \frac{1}{k} (\eta + F_e). \quad (3)$$

We will denote by  $\bar{F} := \frac{1}{k} (\eta + F_e)$  and will be referred to as the normalized force;  $\bar{F}$ , which represents nominal displacement of the bead under the influence of combined force  $\eta + F_e$ .

#### B. Open loop model: Instrumentation dynamics

The optical tweezers instrumentation introduces its own dynamics into the system that has a significant effect on the measurements and the actuator inputs. They are modeled as



follows:

$$u = D\tilde{u}, \quad (4)$$

$$y = x + n, \quad (5)$$

where  $\tilde{u}$  is the desired position of the trap and is also the input to the AOD.  $D$  is the transfer function of instrumentation dynamics that includes the delay introduced by the finite sampling time and response time of AOD.  $y$  is the measurement of the bead position  $x$ , corrupted by noise  $n$ . Thus it follows that

$$y = GD\tilde{u} + G\bar{F} + n. \quad (6)$$

The above equation represents the open loop system where the actuator input,  $\tilde{u}$  is provided by the user instead of being generated by a controller. The transfer function from the input,  $\tilde{u}$  to the output  $y$  is  $GD$ . The corresponding frequency response is shown in Fig. 2.

### C. Closed loop model

In the closed loop operation, the measured output,  $y$ , is processed by a controller to decide the control action,  $\tilde{u}$ . In CPOT, one of the objectives of the controller is to regulate the bead position, where  $y$  is compared with a reference value,  $r$  and the difference between these quantities,  $e := r - y$ , is used by the controller  $K$  to generate a control signal,  $\tilde{u}$ , to reduce the regulation error,  $e_r = r - x$ . Thus,

$$\tilde{u} = K(r - y), \quad (7)$$

and merging Eqs. (3)–(5) and (7), we get a closed loop relation between external inputs and measured output, given by

$$y = \frac{G}{1+L}\bar{F} + \frac{L}{1+L}r + \frac{1}{L}n, \quad (8)$$

where  $L = DKG$ .  $L$  is called the loop gain and constitutes the product of the transfer functions involved in the closed loop operation. We further define the sensitivity transfer function,  $S$ , and the complementary sensitivity transfer function,  $T$ , by

$$S := \frac{1}{1+L}, \quad (9)$$

$$T := \frac{L}{1+L}. \quad (10)$$

Note that  $S + T = 1$ . With these new definitions, Eq. (8) can be rewritten as

$$y = GS\bar{F} + Tr + Sn. \quad (11)$$

The significance of the transfer functions  $S$  and  $T$  is explained later.

## IV. FUNDAMENTAL LIMITATIONS

### A. Emergence of peak

In CPOT operation, the control effort,  $\tilde{u}$  counters the effect of external forces to maintain the bead position at a

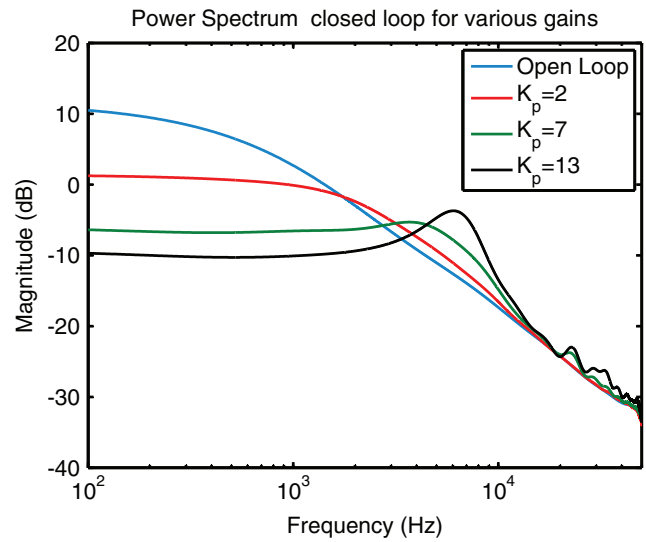


FIG. 3. (Color online) Experimentally obtained power spectrum of the bead position for a  $2.1 \mu\text{m}$  diameter bead for different values of proportional gains,  $k_p$ , in a constant position tweezers configuration. The power spectrums are smoothed for clarity using a polynomial fit. The peaking behavior is distinct for  $k_p = 13$ .

constant value.  $\tilde{u}$  is considered a direct measure of the normalized force,  $\bar{F}$ . A proportional controller increases the effective trap stiffness and thereby increases the bandwidth of force estimation.<sup>7</sup> Indeed, consider the experimentally obtained power spectral density (psd) plots of the bead position shown in Fig. 3 for the open-loop case and for three different cases of closed-loop operation with varying proportional gains  $k_p$ . It is seen that with  $k_p = 2$ , the cut-off frequency (the frequency where the psd starts to roll off) is higher than the open-loop case. This cut-off frequency is related to the temporal resolution of estimating external forces where a higher cut-off frequency results in a higher temporal resolution.<sup>4,11</sup> In Fig. 3 it is also seen that with the proportional gain  $k_p = 7$  and  $k_p = 13$ , the cut-off frequency is higher. However, the resulting psd now deviates from a first order shape due the emergence of a peak. The emergence of a peak in the psd is attributed to the latencies in the closed loop implementation that includes data acquisition sampling and delays within the actuator.<sup>4,7,11</sup> We show that the extent of the peaking behavior can be predicted by the sensitivity transfer function  $S$  of the closed loop system. Furthermore, we also show how the objectives of force estimation and position regulation are related to  $S$  and we delineate fundamental limitations in obtaining desired characteristics in  $S$ .

### B. Limitations explained using $S$

With perfect regulation, i.e.,  $y = r$ , we have  $S = 0$  and  $T = 1$ , which is easily deduced from Eq. (11). Under these conditions, the trap movement,  $u$  is such that it cancels all the external force disturbances and thus  $u$  becomes an estimate of the normalized external force,  $\bar{F}$ . The requirement,  $S = 0$ , is uniform over all the frequencies,  $\omega$ . The question then arises: is it possible to make  $S = 0$ ? The short answer is “No.” The reason is explained

as follows. Note that  $S = \frac{1}{1+DKG}$ , where  $D$  models the dynamics of AOD. Latencies in a system result in a transfer function containing right half plane (RHP) zeros.<sup>4,7</sup> As expected, experimentally identified  $D$  (see experimental results,  $D = 0.86 \frac{(s+111)^2(s^2-1.61 \times 10^5 s + 1.1 \times 10^{10})}{(s+1167)(s^2+1.5 \times 10^5 s + 9 \times 10^9)}$ ) does contain RHP zeros that result from latencies in the AOD. Presence of RHP zeros can lead to emergence of a peak in psd when proportional controller gain,  $k_p$  is increased, which we demonstrate next. The weighted sensitivity integral formula (also called the second waterbed formula)<sup>13</sup> states that  $\int_0^z \ln |S(j\omega)| d\omega \approx \text{constant}$ , where  $z$  is the frequency of the RHP zero. In other words, the area under the logarithm plot of magnitude of sensitivity transfer function,  $S$ , within a finite frequency region,  $[0, z]$ , is a constant. The theorem on this result is provided in the supplementary material.<sup>16</sup> The width of the frequency region is dictated by the location of RHP zeros of  $L$  whereas the constant depends on the location of both the RHP poles and the zeros of  $L$ . Closer the RHP zero is to 0, smaller the frequency region. A PI controller is designed to reduce the magnitude of  $S$ , within a frequency region  $[0, \omega_B]$ . It successfully achieves this but at the cost of increasing  $S$  in the higher frequency range (to maintain a constant area) which affects the spectrum of bead position, given by

$$\text{psd}_x(\omega) = \frac{1}{2\pi} |G(\omega)|^2 |S(\omega)|^2 \text{psd}_{\bar{F}},$$

where  $\text{psd}_x$  and  $\text{psd}_{\bar{F}}$  are the psds of the bead position,  $x$  and that of the normalized external force,  $\bar{F}$ , respectively. The lower bound on the magnitude of the peak in the psd, i.e.,  $\|S\|_\infty$ , also depends on the location of RHP zero in the loop transfer function,  $L$ .<sup>14</sup> Smaller the magnitude of RHP zero, greater the lower bound on  $\|S\|_\infty$  (see supplementary material<sup>16</sup> for the theorem on this result). As  $|S|$  is reduced for certain frequency range,  $\|S\|_\infty$  increases. Thus, it is impossible to avoid emergence of peak in the power spectrum of trapped bead position (or equivalently increase the bandwidth of optical tweezers for external force estimation) for any linear controller  $K$ . In summary we have identified latencies in the instrumentation dynamics as the primary bottleneck to high bandwidth force estimation with analytical estimates on the bandwidth possible and the maximum magnitude of the regulation error (given by the peak in  $|S|$ )

## V. CONTROL STRATEGY

### A. System inversion

As shown in Sec. IV B, RHP zeros imposes fundamental limitations on increasing the bandwidth of CPOT as a force probe. This challenge was partly met by Sehgal *et al.*<sup>7</sup>, where the objectives of constant position regulation and estimation of  $\bar{F}$ , were addressed independently. A proportional-integral controller,  $K^{PI}$ , was designed for position regulation. The external forces were estimated by inverting the transfer function relating  $\bar{F}$  to  $y$ , which is modeled as  $y = GS\bar{F}$  (from Eq. (11)). In this scheme, an inverted system,  $K_2^{PI} = (GS)^{-1}$  was designed to process the measurement,  $y$  and generate an estimate,  $\hat{\bar{F}}$  of actual  $\bar{F}$ . The drawback of this scheme is that

the controller,  $K^{PI}$ , is not optimal and the approach of system inversion is *ad hoc* which is not optimized with respect to the controller. Furthermore, inverting the transfer function from  $\bar{F}$  to  $y$  is sensitive to any uncertainty in modeling.

### B. Robust control

In this section, various performance objectives related to constant position regulation and estimation of forces are identified and an optimal strategy based on robust control theory is developed. The result is a further increase in the bandwidth of external force estimation over the system-inversion method. The objectives of the robust controller are outlined below:

1. The primary objective of the controller is yield a good estimate,  $\hat{\bar{F}}$ , of normalized external force,  $\bar{F}$ .
2. Another objective for the controller is maintaining the bead position at a constant desired value.
3. The third objective is to avoid large trap movements,  $u$ , to maintain the validity of linear spring assumption of the optical trap and thereby avoid instabilities in the system (arising out of non-linearities).

These objectives can be mutually conflicting and therefore an optimization based strategy is required that achieves these objectives in a balanced manner. In this article, such an optimal strategy is developed using the robust control framework. A single-input, multi-output controller structure is adopted where the input is error in regulation,  $e_r$  and outputs are control signal,  $\tilde{u}$  and force estimate,  $\hat{\bar{F}}$ . Written compactly,  $[\tilde{u} \ \hat{\bar{F}}]^T = K e_r$ , with  $K = [K_1 \ K_2]^T$ . The idea is to generate a control signal,  $\tilde{u}$ , using  $K_1$  and to generate an estimate,  $\hat{\bar{F}}$ , using  $K_2$ . The multiple objectives of constant position regulation, bounded trap movement (or control effort), and estimation of external force are mathematically described by the following relations:

$$\begin{aligned} |e_r(\omega)| &< |W_s^{-1}(\omega)\bar{F}(\omega)| \text{ or } |W_s \frac{e_r}{\bar{F}}| < 1 \text{ for all } \omega, \\ |u(\omega)| &< |W_u^{-1}(\omega)\bar{F}(\omega)| \text{ or } |W_u \frac{u}{\bar{F}}| < 1 \text{ for all } \omega, \\ |e_F(\omega)| &< |W_F^{-1}(\omega)\bar{F}(\omega)| \text{ or } |W_F \frac{e_F}{\bar{F}}| < 1 \text{ for all } \omega, \end{aligned} \quad (12)$$

where  $e_F := \bar{F} - \hat{\bar{F}}$  is the error in the estimation of force,  $\bar{F}$  and the three requirements in Eq. (12) correspond to position regulation, providing bounds on trap movement and force estimation, respectively.  $W_s$ ,  $W_u$ , and  $W_F$  are the weighting transfer functions provided by the control designer to emphasize the relative importance of the frequencies for which the objective is to be met. The magnitude of weighting functions must be large for frequencies where smaller magnitudes are desired (so that the desired error bound reduces). As explained in Sec. IV B, error at all frequencies cannot be reduced simultaneously, therefore, an insightful choice of weighting functions is required from the control designer. More on how to choose these transfer functions is discussed in Sec. VI. Next, we derive alternate relations for performance objectives in terms of transfer functions. The transfer functions  $\frac{e_r}{\bar{F}}$ ,  $\frac{u}{\bar{F}}$ ,  $\frac{e_F}{\bar{F}}$  in Eq. (12), can be evaluated from the previous equations as

given below:

$$\begin{aligned}\frac{e_r}{\bar{F}} &= GS^R, \\ \frac{u}{\bar{F}} &= -T^R, \\ \frac{e_F}{\bar{F}} &= 1 + K_2GS^R,\end{aligned}\quad (13)$$

where

$$S^R = \frac{1}{1 + L^R}, \quad (14)$$

$$T^R = \frac{L^R}{1 + L^R}, \quad (15)$$

$$L^R = K_1DG. \quad (16)$$

In deriving Eq. (13), we have assumed  $r = 0$  and  $n = 0$ , which are non-restrictive assumptions but simplify the problem significantly. Thus, the objectives in Eq. (12) are equivalently described by the following conditions:

$$\begin{aligned}\|W_sGS^R\|_\infty &< 1, \\ \|W_uT^R\|_\infty &< 1, \\ \|W_F(1 + K_2GS^R)\|_\infty &< 1.\end{aligned}\quad (17)$$

These conditions can be represented by a single matrix inequality,

$$\left\| \underbrace{\begin{bmatrix} W_sGS^R \\ W_uT^R \\ W_F(1 + K_2GS^R) \end{bmatrix}}_M \right\|_\infty < 1. \quad (18)$$

The optimal control problem is to synthesize a transfer function matrix  $K(s) = [K_1(s)K_2(s)]^T$  such that the H-infinity norm of the performance objective transfer function matrix,  $M$  is minimized. The controller transfer function  $K_1$  alone achieves the performance objectives of constant position regulation and bounded control input, while the transfer function  $K_2$  aids the minimization of the estimation error,  $e_F$ , in conjunction with  $K_1(s)$ . The estimation error,  $e_F$ , is required to be small for a large frequency range to achieve a high bandwidth estimation of the external force input,  $\bar{F}$ . The estimate

$\hat{F}$  is filtered with an appropriately designed Wiener filter to minimize the contribution due to thermal noise.

## VI. RESULTS AND CONCLUSIONS

In this section we present the analytical and experimental results obtained by implementing the control strategy developed in Sec. V B. These results are also compared with the results obtained using the method of system inversion<sup>7</sup> showing the benefits of robust control methodology. An optical trap was created for a polystyrene bead of diameter  $2.1 \mu\text{m}$ . The parameters of the transfer function,  $G = k/(\beta s + k)$  were found experimentally using the power spectrum method.<sup>15</sup> The spring constant  $k$  was determined to be  $0.02 \text{ pN nm}^{-1}$ . The drag coefficient  $\beta$  was chosen to be  $1.76 \times 10^{-5} \text{ N s m}^{-1}$ , corresponding to that of water at  $25^\circ\text{C}$ . This resulted in a cut-off frequency,  $f_c = k/2\pi\beta$ , for  $G$  to be  $176 \text{ Hz}$ . The transfer function,  $H$ , relating  $\tilde{u}$  and  $y$  was experimentally determined using the frequency sweep method.<sup>4,7</sup> The frequency response is shown in Fig. 2(a).  $H$  was fitted with a 2 zeros and 3 poles model. As expected,  $H$  has RHP zeros, which imposes a fundamental limitation (see Sec. IV). Note that  $H = DG$ , therefore, the instrumentation dynamics,  $D$  can be evaluated using the relation:  $D = H/G$ . The deduced frequency response of  $D$  is shown in Fig. 2(b). After finding analytical models for the individual transfer functions, the external force input was estimated using the method of system inversion<sup>7</sup> and the proposed robust control method.

### A. System-inversion approach

For the system-inversion method, the PI gains,  $k_p$  and  $k_i$ , were chosen to minimize the output variance ( $y^2$ ). They were found to be  $k_p = 10$  and  $k_i = 10000$ . The PI controller is represented as  $K^{PI} = k_p + k_i/s$ . The corresponding closed-loop sensitivity and complementary-sensitivity transfer functions are denoted by  $S^{PI}$  and  $T^{PI}$  where the superscript,  $PI$ , is introduced to distinguish them from the transfer functions obtained in the robust control framework. Using the system inversion approach,  $K_2^{PI}$  is synthesized as  $\frac{-1}{GS^{PI}} \frac{2\pi f_Q}{(1+2\pi f_Q)}$ , where  $GS^{PI}$  is the transfer function relating  $\bar{F}$  to  $y$ . The low pass filter  $2\pi f_Q/(s + 2\pi f_Q)$  is introduced for convenience in digital implementation of  $K_2^{PI}$  ( $GS^{PI}$  is an improper transfer function<sup>7</sup>).

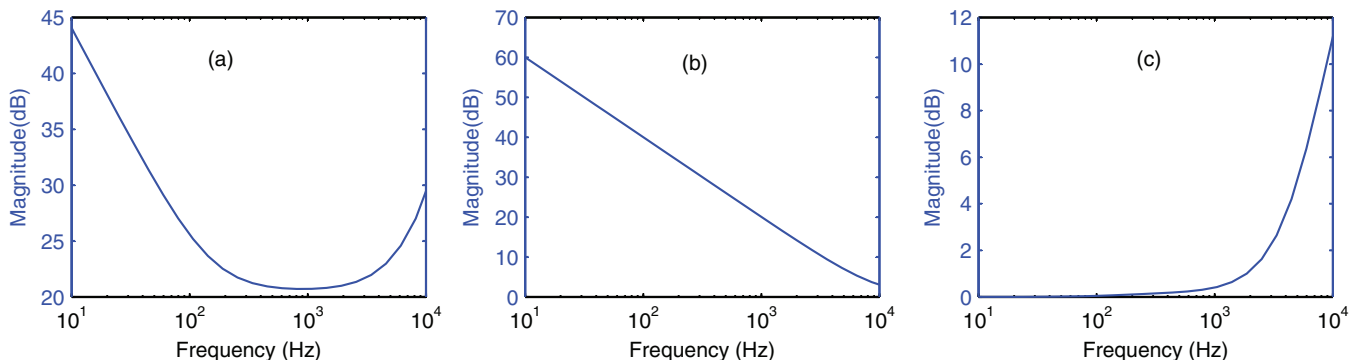


FIG. 4. (Color online) Magnitude of frequency responses of the weighting functions. (a)  $W_s$ , weight on regulation error. (b)  $W_F$ , weight on force estimation error. (c)  $W_u$ , weight on controller effort.

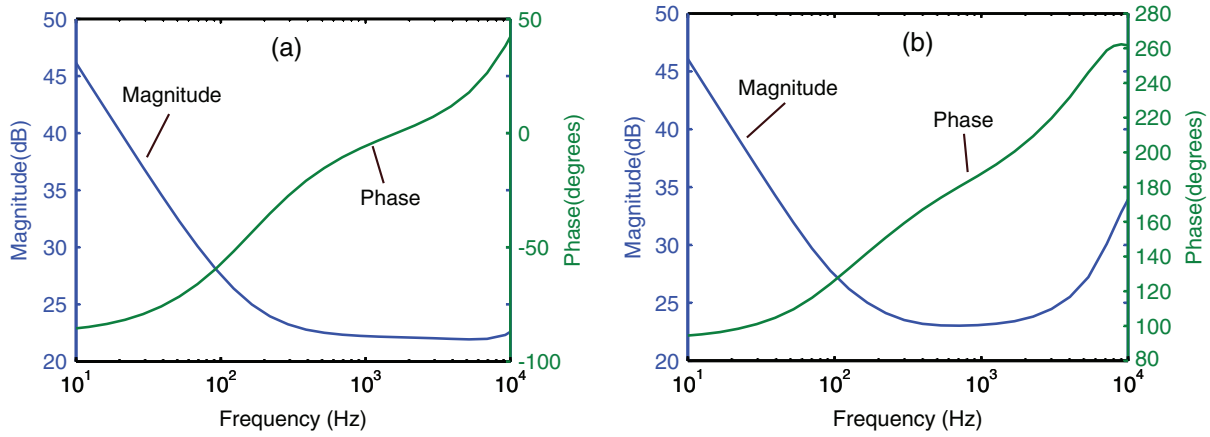


FIG. 5. (Color online) Frequency response of the robust controller transfer functions. (a)  $K_1$ : primarily achieves position regulation objective while keeping control effort within limits. (b)  $K_2$ : output of this part of the controller is an estimate of the external force,  $F_e$ .

## B. Robust control approach

The goal of synthesizing optimal filters  $K_1$  and  $K_2$  to meet the three performance objectives listed in Sec. V depends on a careful choice of the weighting functions,  $W_s$ ,  $W_u$ , and  $W_F$ . These weighting functions were designed by utilizing the best PI controller,  $K^{PI} = 10 + 10\,000/s$  as,

$$\begin{aligned} W_s &= (GS^{PI})^{-1}, \\ W_u &= (T^{PI})^{-1}, \\ W_F &= (1 + K_2^{PI}GS^{PI})^{-1}. \end{aligned}$$

All RHP poles in these weighting functions were transposed to the left half plane (reversed the sign of the real part of the pole) to keep the magnitude plot of these transfer functions unchanged. Purely imaginary poles (real part of pole equal to zero) in these weighting functions were replaced by a pole at  $-1$  in LHP. Frequency responses of the weighting functions are shown in Fig. 4 and the frequency response of the controller  $K = [K_1 \ K_2]^T$  is shown in Fig. 5. The  $K$  that minimizes  $\|M\|_\infty$  is optimal among the class of all linear stabilizing controllers. The controller  $K_1$  was implemented in real time on National Instruments real-time FPGA. For the estimation of the external input force,  $\bar{F}$ , the high order filter  $K_2$  was im-

plemented offline. A time trace of the bead position with and without the control action is shown in Fig. 6 that confirms the stability of the controller and verifies the position regulation objective.

## C. Comparison

The regulation performance objective was defined through the condition  $\|W_s GS^R\|_\infty < 1$ , (Eq. (17)). This is alternatively expressed by the condition,  $|GS^R(\omega)| < |W_s^{-1}(\omega)|$  for all  $\omega$ . In other words, the magnitude part of the frequency response of  $GS^R$  should lie below that of  $W_s^{-1}(\omega)$ . Figure 7(a) shows that the robust controller meets this condition better than the PI controller because  $|GS^R(\omega)| < |GS^{PI}(\omega)| < |W_s^{-1}(\omega)|$  for all  $\omega$ . Similar analysis was done for the objective of bounded controller effort, i.e.,  $\|W_u GK_1 DS^R\|_\infty < 1$ . Figure 7(b) shows that both controllers meet the objective. In this case, control effort of the robust controller is almost the same as that of PI controller except at higher frequencies where robust controller is slightly more aggressive.

As mentioned earlier, the estimation of external force input remains the most important performance objective of CPOT. Figure 8(a) shows the results for force estimation objective, i.e.,  $\|W_F(1 + K_2 GS^R)\|_\infty < 1$ . Magnitude of error in force estimation by the robust controller is at least 10 dB below that by the system-inversion method for all frequencies up to 10 kHz. This confirms that using robust controller transfer functions  $K_1$  and  $K_2$  can help increase force estimation bandwidth of optical tweezers over the method of system inversion. System-inversion method was previously shown to be an order in magnitude better (in terms of bandwidth) than the conventional method of force estimation.<sup>7</sup> This claim is further confirmed by looking at the frequency response of transfer function between external force input,  $\bar{F}$ , and its estimate,  $\hat{F}$ , shown in Fig. 8(b). The transfer function from  $\bar{F}$  to  $\hat{F}$  remains very close to unity for the robust control method (up to 10 kHz) and for system inversion, it stays within the  $-3$ dB specification. In contrast, phase plot of system-inversion approach, falls rapidly beyond 2 kHz. This indicates the estimate,  $\hat{F}$ , obtained using the system inversion

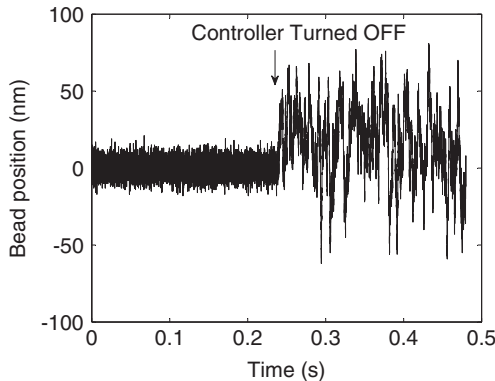


FIG. 6. Time trace of bead position with and without the robust controller. The controller is turned off at the indicated time whereafter the Brownian excursions of the bead within the trapping potential can be clearly seen to be much larger than the feedback controlled portion.



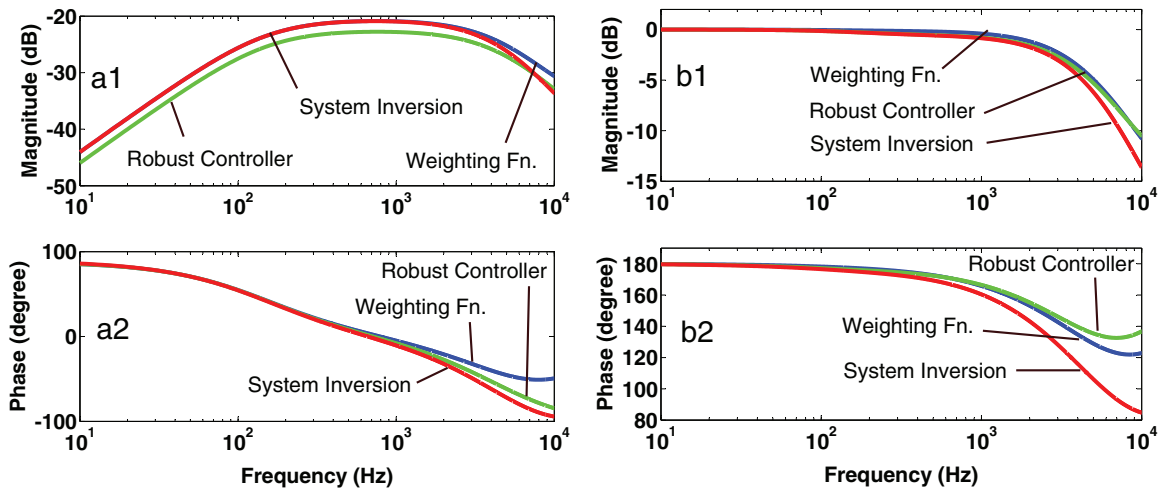


FIG. 7. (Color online) (a1) Verification of the first performance objective:  $|W_s e_r| < 1$ , or, the magnitude of error in position regulation,  $e_r$  is smaller than the chosen weighting function  $W_s^{-1}$  for all the frequencies. (a2) Phase part of the frequency response from external force,  $\bar{F}$  to regulation error,  $e_r$ . No bound on phase response was specified. (b1) Verification of the second performance objective:  $|W_u u| < 1$ , or, the magnitude of control effort,  $u$  is within the limits specified by the weighting function,  $W_u$ . (b2) Phase part of the frequency response from external force,  $\bar{F}$  to control effort,  $u$ .

approach is not a good reflection of  $\bar{F}$ , if it has frequency content above 2 kHz.

The analytical results obtained for the robust control method and the system inversion approach were confirmed by experimental data. Experimental data were generated by first adding a sinusoidal frequency sweep (chirp) signal,  $d$  to  $\tilde{u}$ . The effect of this signal is to disturb the trap position by  $Dd$ . This corresponds to normalized external force  $\bar{F}$ . Amplitude of the disturbance signal was set to 100 nm. With this disturbance active, the error signal,  $e_r$  and estimated signal,  $\hat{F}$  were recorded. Frequency response was subsequently obtained by computing the ratio of Fourier transforms of the signals. Multiple datasets were recorded to average out the effect of thermal noise. Figure 9(a) shows the experimentally obtained frequency response of the transfer function between  $\bar{F}$  and

$e_r$  using the two methods and was found in good agreement with the analytically obtained transfer functions shown in Fig. 7(a). Figure 9(b) compares the experimentally obtained plot between the external force input,  $\bar{F}$  to its estimate,  $\hat{F}$ , for the two methods. We see that the magnitude plot of transfer function remained within 3 dB range up to  $\sim 6.5$  kHz for both the methods. However, the phase remained within  $\pm 15^\circ$  up to 7.5 kHz for the robust control method and up to 2 kHz for the system inversion scheme. Thus, experimentally it was observed that the robust control method helped improve bandwidth of estimation of external force input by over three times. We would like to remark that the physical model,  $G$ , for the optical tweezers was chosen to be based on simple first order dynamics that ignores higher order effects of hydrodynamic forces. A more accurate analysis that includes such effects is

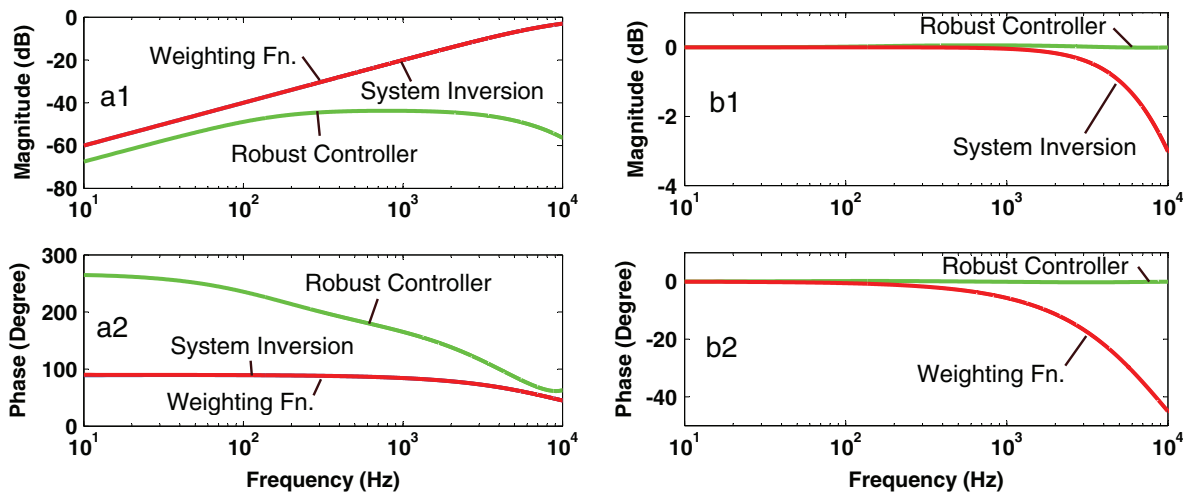


FIG. 8. (Color online) (a1) Verification of the third performance objective:  $|W_F e_F| < 1$ , or, the magnitude of error in force estimation,  $e_F$  is less than that specified by the weighting function  $W_F^{-1}$  for all frequencies. (a2) Phase part of the frequency response from external force,  $\bar{F}$  to estimation error,  $e_F$ . No bounds on phase response was specified. (b1) Comparison of robust control and system inversion methods in estimation of force,  $\bar{F}$ . Magnitude of ratio of force estimate,  $\hat{F}$  to actual force,  $\bar{F}$  is shown for the robust control method and for the system inversion method. Estimates from the robust control method matches well with the actual force even for higher frequencies which is not the case for the system inversion method. (b2) Comparison of the two methods in the lag associated with estimation. System inversion method has higher lag compared to the robust control method especially at higher frequencies.

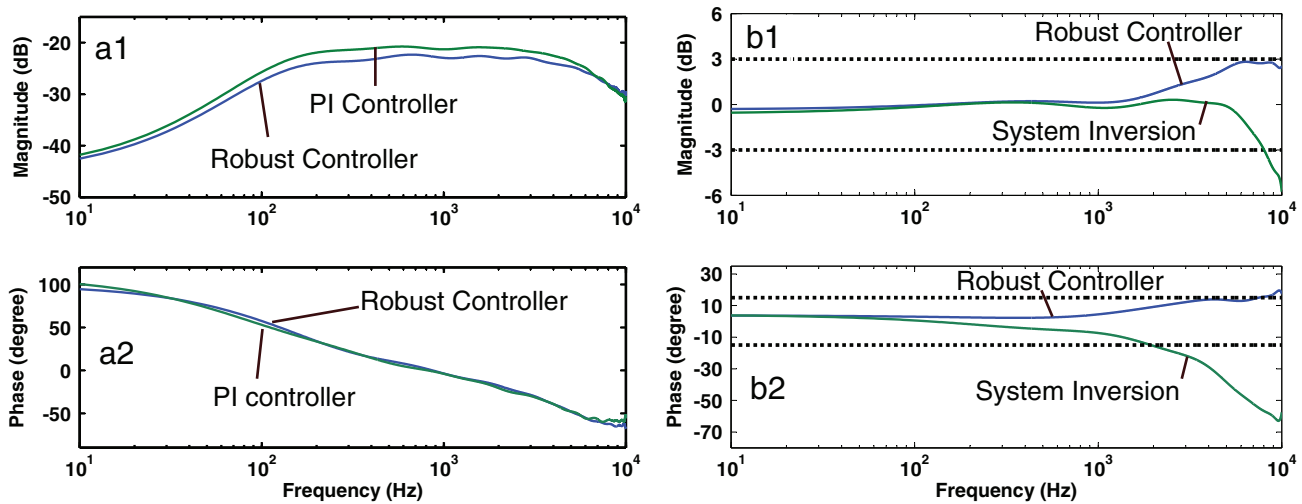


FIG. 9. (Color online) (a1) Experimental verification of the performance objective to maintain the bead position,  $x$  at zero. Plots show the magnitude part of the transfer function from external force,  $\bar{F}$  to regulation error,  $e_r$ . The robust control method achieves slightly better regulation compared to the PI controller. (a2) Phase part of the frequency response. Both controllers offer similar performance in phase response. (b1) Experimental verification of the performance objective to estimate external force,  $\bar{F}$ . Plots show magnitude part of the frequency response of the transfer function from external force,  $\bar{F}$  to its estimate  $\hat{F}$  using the robust control method and the system inversion method. The two methods perform similarly for all frequency in estimating force magnitudes. (b2) The two methods differ in the corresponding phase response. Estimates by the system inversion method has significant phase lag compared to that obtained by the robust control method, for frequencies beyond 1.5 kHz.

provided by Ref. 5. Note however, that the modern control methodology, unlike the traditional PI design, incorporates the model of the system to determine the optimal controller. Thus, the models used need to be tractable for the controller design process. Also, the complexity of the optimal controller determined depends on the complexity of the models of the system involved and thus even if the control design process determines a controller, the real-time task of implementing the controller can be thwarted by a overly complex controller. That said, if these challenges can be overcome then a better system model will yield better performance. Thus, the strategy of control design outlined in this article can be adopted for better models with further enhancements in the performance of optical tweezer operation, which is a part of future work. The efficacy of the controller design presented here can be partly assessed by the experimental results in Fig. 6 where the bead motion due to thermal noise when the controller is on and off is shown.

<sup>1</sup>S. Chu, J. Bjorkholm, A. Ashkin, and A. Cable, *Phys. Rev. Lett.* **57**, 314 (1986).

<sup>2</sup>S. Block, L. Goldstein, and B. Schnapp, *Nature* **348**, 348 (1990).

<sup>3</sup>J. Finer, R. Simmons, and J. Spudich, *Nature (London)* **368**, 113 (1994).

<sup>4</sup>H. Sehgal, T. Aggarwal, and M. Salapaka, *Proc. SPIE* **7038**, 703831 (2008).

<sup>5</sup>K. Berg-Sørensen and H. Flyvbjerg, *Rev. Sci. Instrum.* **75**, 594 (2004).

<sup>6</sup>K. Visscher, M. Schnitzer, and S. Block, *Nature (London)* **400**, 184 (1999).

<sup>7</sup>H. Sehgal, T. Aggarwal, and M. Salapaka, *Appl. Phys. Lett.* **94**, 153114 (2009).

<sup>8</sup>J. Moffitt, Y. Chemla, S. Smith, and C. Bustamante, *Biochemistry* **77**, 205 (2008).

<sup>9</sup>J. Wen, M. Manosas, P. Li, S. Smith, C. Bustamante, F. Ritort, and I. Tinoco, Jr., *Biophys. J.* **92**, 2996 (2007).

<sup>10</sup>W. Greenleaf, M. Woodside, and S. Block, *Ann. Rev. Biophys. Biomol. Struct.* **36**, 171 (2007).

<sup>11</sup>A. Wallin, H. Ojala, E. Hægström, and R. Tuma, *Appl. Phys. Lett.* **92**, 224104 (2008).

<sup>12</sup>R. Simmons, J. Finer, S. Chu, and J. Spudich, *Biophys. J.* **70**, 1813 (1996).

<sup>13</sup>S. Skogestad and I. Postlethwaite, *Multivariable Feedback Control: Analysis and Design* (Wiley, New York, 1996).

<sup>14</sup>J. Freudenberg and D. Looze, *IEEE Trans. Autom. Control* **30**, 555 (2002).

<sup>15</sup>K. Visscher, S. Gross, and S. Block, *IEEE J. Sel. Top. Quantum Electron.* **2**, 1066 (2002).

<sup>16</sup>See supplementary material at <http://dx.doi.org/10.1063/1.3660271> for notes on robust control paradigm, theorem statements, and details of transfer functions obtained.